Langmuir

Article

pubs.acs.org/Langmuir

Molecular Dynamics and Energy Landscape of Decanethiolates in Self-Assembled Monolayers on Au(111) Studied by Scanning Tunneling Microscopy

Kai Sotthewes,[†,§] Hairong Wu,[†,‡,§] Avijit Kumar,[†] G. Julius Vancso,[‡] Peter M. Schön,[‡] and Harold J. W. Zandvliet*[,†]

[†]Physics of Interfaces and Nanomaterials and [‡]Materials Science and Technology of Polymers, MESA+ Institute for Nanotechnology, University of Twente, Post Office Box 217, 7500AE Enschede, The Netherlands

ABSTRACT: The energetics and dynamics of the various phases of decanethiolate self-assembled monolayers on Au(111) surfaces were studied with scanning tunneling microscopy. We have observed five different phases of the decanethiolate monolayer on Au(111): four ordered phases (β, δ, χ^*, and ϕ) and one disordered phase (ε). We have determined the boundary free energies between the disordered and order phases by analyzing the thermally induced meandering of the domain boundaries. On the basis of these results, we are able to accurately predict the two-dimensional phase diagram of the decanethiolate/Au(111) system. The order−disorder phase transition of the χ^* phase occurs at 295 K, followed by the order−disorder phase transition of the β phase at 325 K. Above temperatures of 325 K, only the densely packed ϕ and disordered ε phases remain. Our findings are in good agreement with the phase diagram of the decanethiolate/Au(111) system that was put forward by Poirier et al. [*Langmuir* **2001**,*17* (4), 1176−1183].

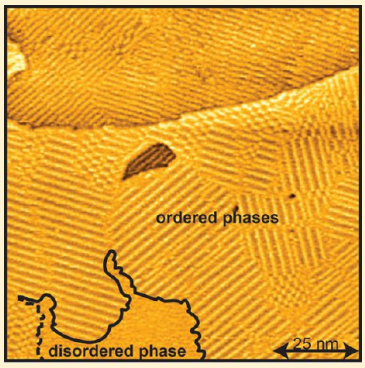

INTRODUCTION

Molecular self-assembly is omnipresent in nature: it is of key importance for many biological processes.[1−4] Self-assembly of organic molecules into highly ordered monolayer films on metal or semiconductor surfaces has potential applications in molecular electronics, biosensing, corrosion inhibition, and biomimetics.[5−8] It is well-known that alkanethiols form well-ordered self-assembled monolayers (SAMs) on Au(111) surfaces.[9−13] The relative ease of fabrication of alkanethiol SAMs has led to many studies and potential applications.[14−17] In particular, the decanethiol self-assembled monolayer on Au(111) has served as a prototypical model system for self-assembly.[1,18−22] Upon adsorption, the decanethiol molecule is deprotonated and thus becomes a decanethiolate.

The formation of self-assembled monolayers is governed by a number of parameters, such as temperature, substrate morphology, coverage, and crystal structure.[4,21] The formation of decanethiolate SAMs on Au(111) was extensively studied by Poirier et al.[1,22−24] On the basis of a detailed experimental study, these authors have put forward a two-dimensional phase diagram of the decanethiolate/Au(111) system.[1] They found that decanethiolates can order into different phases: a phase where the tails of the decanethiolate molecules are in an upright position and tilted 30° from the surface normal (ϕ phase), a disordered liquid- or gas-like phase (ε),[26] and three phases where the decanethiolate molecules are lying flat on the surface (β, δ, and χ). The most densely packed phase, the ϕ phase, is dominant at high coverage ($>{}^1/_3$ monolayer) and exhibits a c(3 × $2\sqrt{3}$)R30° registry, whereas the flat-lying and disordered phases are found at coverage lower than ${}^1/_3$ monolayer.[13,22] The β phase is a striped phase where the decanethiolate molecules lie flat on the surface in an alternating head-to-head and tail-to-tail registry.[25] The δ phase is very comparable to the β phase; however, the tails of the decanethiolate molecules partly lie on top of each other, leading to a denser packed structure. The χ phase consists of a perfect array of alternating β and δ stripes.[22] Toerker et al.,[27] and later also Li et al.,[28] found in the low-coverage regime a new phase, referred as the χ^* phase. The χ^* phase is also composed of β and δ domains; however, in contrast to the χ phase, the width of the β and δ domains varies from location to location.

Despite numerous studies, a full understanding of the decanethiolate/Au(111) system has not yet been achieved. One issue that is still not completely solved deals with the thermodynamic stability of the different domains.[29]

The goal of this study is to investigate the occurrence and thermal stability of the different ordered phases of a decanethiolate SAM on Au(111) by analyzing the domain boundaries between the phases. We will focus in particular on the domain boundaries between the low-coverage ordered phases and the disordered phase. By a statistical analysis of the thermally induced domain wandering, we will be able to derive the two-dimensional phase diagram for this system. The boundary free energy between the χ^* and ε phases and between the β and ε phases vanishes at 295 and 325 K, respectively. These transition temperatures are in very good

Received: January 8, 2013
Revised: February 18, 2013
Published: February 20, 2013

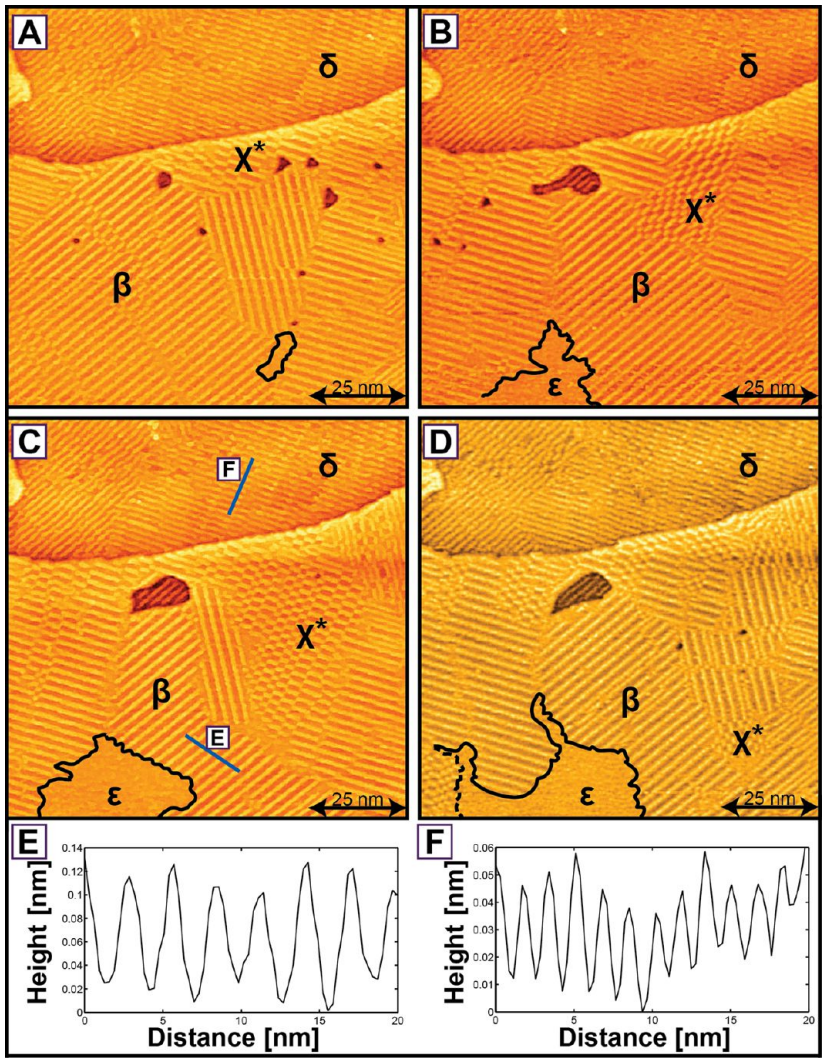

Figure 1. (A–D) Sequence of STM images (100 nm × 100 nm) showing dynamic behavior of a decanethiolate SAM on the Au(111) at room temperature (293 K). The surface exhibits three ordered phases (β, δ, and χ^*) and one disordered phase (ε). The solid line marks a domain boundary between the ordered β phase and the disordered ε phase, while the dashed line marks a $\chi^*-\varepsilon$ domain boundary. The sample bias is 1.2 V and the tunnel current is 190 pA. The time lapse between consecutive images is 420 s. (E, F) Line profiles taken across the β and δ phases, respectively. The stripe widths are (E) 3.3 nm and (F) 2.2 nm.

agreement with the two-dimensional phase diagram proposed by Poirier et al.[1]

EXPERIMENTAL SECTION

Substrates were purchased from Arrandee (Werther, Germany) and contain a 250 nm Au/2 nm Cr layer on borosilicate. The substrates were flame-annealed in high-purity H_2 gas for 5 min. After flame annealing, the samples were inserted in an ultrahigh vacuum system with a base pressure of 1×10^{-10} mbar and then imaged with a scanning tunneling microscope (STM; RHK Technology, Troy, MI). The surface exhibited the characteristic Au(111) herringbone structure. Subsequently the samples were taken out of the ultrahigh vacuum (UHV) system. Self-assembled decanethiol (Sigma–Aldrich, Steinheim, Germany) monolayers on the Au(111) surface were produced by immersing the samples into a dilute 1 mM 1-decanethiol in ethanol solution for 24 h. This immersion step leads to a densely packed SAM where the decanethiolate molecules form a standing-up phase. In order to reduce the coverage of the decanethiolate molecules, we immersed our sample in a pure ethanol solution for 1 h. Subsequently the samples were loaded into the UHV STM for imaging. In order to prevent damage of the self-assembled monolayer, STM images were recorded at sample biases less than 1.2 V and tunneling currents less than 190 pA.[23,30] The temperature in the laboratory was kept constant at 293 ± 1 K.

RESULTS AND DISCUSSION

In Figure 1, four consecutive scanning tunneling microscopy (STM) images of a decanethiolate SAM on Au(111) are shown. The SAM consists of three ordered phases (β, δ, and χ^*) and one disordered phase (ε). At some regions on the surface, the upright ϕ phase is also present (not shown here). This phase has the highest packing density and exhibits a $c(3 \times 2\sqrt{3})R30°$ registry. Since we are interested in the low-coverage regime and the ϕ phase is usually found only at higher coverage, we do not consider this phase nor its boundaries here. The only low-density ordered phases adjacent to the ε phase are the β and χ^* phases. The absence of domain boundaries between the δ and ε phases at room temperature suggests that this boundary free energy vanishes at a temperature below room temperature. This does not necessarily imply that the δ phase is completely absent on the surface, since δ phases encapsulated between other ordered domains and/or steps can still be stable.

dx.doi.org/10.1021/la400082z | Langmuir 2013, 29, 3662–3667

The various phases that we observe here were extensively discussed by Poirier.[22] Here we only briefly review these key results and show that our STM data are in excellent agreement with the structural models that were put forward by Poirier.

The β phase is a striped phase consisting of decanethiolate molecules lying flat on the Au(111) surface in an alternating head-to-head and tail-to-tail registry (see Figure 2). The head-to-head pairs align themselves in kinkless rows that form the higher part of the striped phase. The tails of the molecules form the lower part, or troughs, of the striped phase. The corrugation measured along the row direction is 0.5 nm, whereas the periodicity perpendicular to the stripes is 3.3 nm, leading to a c(23 × $\sqrt{3}$) periodicity.[25] The δ phase is very comparable to the β phase; however, the tails of the molecules are lying partly on top of each other, leading to a smaller stripe width of only 7.5 times the nearest-neighbor Au−Au distance, or 2.2 nm, leading to a (5$\sqrt{3}$ × $\sqrt{3}$)R30° periodicity (see Figure 2).[22,26] The measured depth of the troughs is about 0.1 nm for the β phase and only 0.05 nm for the δ phase (see Figure 1E, F). The measured trough depths are consistent with the above-discussed structural models of the β and δ phases. The χ* phase is a mixture of small β and δ domains with stripe widths of 3.3 or 2.2 nm, respectively. The χ* phase shows switching behavior between the stripe segments, suggesting that this phase is highly dynamic at room temperature.[27] The disordered ε phase does not exhibit any structure, and height profiles taken across several domain boundaries suggest that the decanethiolate molecules are lying flat on the Au(111) substrate.

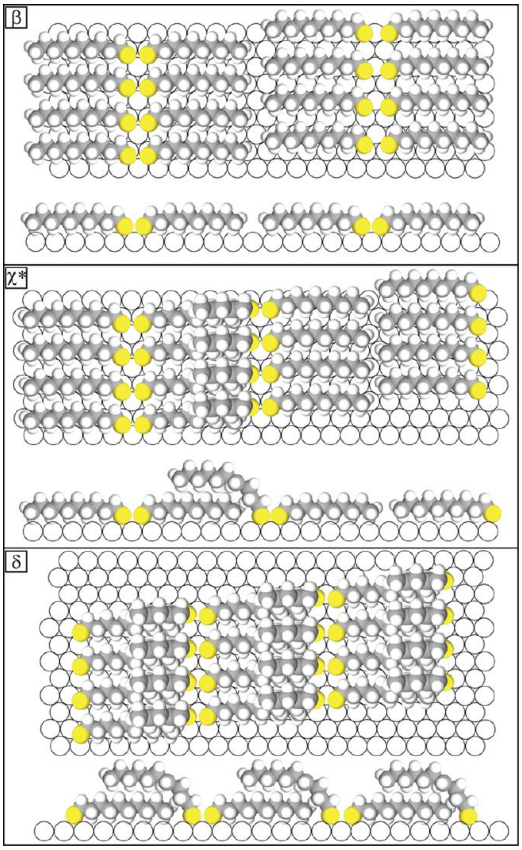

Figure 2. Schematic representation of top and side views of β, χ*, and δ phases. The exact nature of the Au−decanethiolate complex is not yet known and for the sake of simplicity represented here by a simple bond between a sulfur atom and a Au atom of the Au(111) substrate.

Figure 1A shows the coexistence of the four different phases described above. The lower terrace is completely covered with the δ phase and remains stable during the whole experiment. The upper terrace shows several β and χ* domains. In the middle of the upper terrace a large β domain is present surrounded by several smaller χ* domains. Consecutive images recorded with a time interval of 7 minutes (Figure 1B−D) of the same region reveals that the lower terrace remains unaltered during imaging, while the upper terrace is very dynamic. Larger regions convert from β to χ* phase or vice versa. The vacancy islands also exhibit quite some dynamics. In agreement with earlier observations by, for instance, Poirier,[24] the vacancy islands prefer a triangular shape and have a depth of exactly one Au layer. In the vast majority of cases, one finds a well-ordered β phase in the vacancy islands.

A straightforward way to characterize an order−disorder phase transition is via the boundary free energy. At zero temperature, it costs energy to create a domain boundary. With increasing temperature, kinks will be thermally generated in the domain boundary, leading to an increase of the meandering of the boundary. The creation of a kink will cost energy, but the kink can be generated in many different ways, resulting in an increase of the entropy and thus a decrease of the free energy. The order−disorder phase transition occurs at a temperature where the boundary free energy vanishes. As we will show, the domain boundary free energy can be extracted from a statistical analysis of the thermally induced meandering of the domain boundary.

The Au(111) surface has a hexagonal structure with 3-fold symmetry. This 3-fold symmetry shows up in all ordered phases, and therefore we will analyze the meandering of the domain boundaries within the framework of a simple triangular lattice with a nearest-neighbor distance a_{nn} and an isotropic nearest-neighbor interaction energy E.[32,33]

We will start by deriving an expression for the partition function, Z, of an elementary boundary segment. The total partition function of the boundary consisting of N elementary boundary segments is $Z_{total} = Z^N$. The boundary free energy is defined as $F_{total} = -k_bT \ln (Z_{total}) = -k_bT \ln (Z^N) = -Nk_bT \ln (Z) = NF$, where F is the boundary free energy per elementary boundary segment, k_b is the Boltzmann constant, and T is temperature.

The formation of an elementary boundary segment with unit length $a_{nn}\sqrt{3}/2$ along one of the three high-symmetry directions involves the breaking of two nearest-neighbor bonds (see Figure 3). For the sake of simplicity, we take from now on $a = a_{nn}\sqrt{3}/2$ as our elementary length unit. The formation energy of an elementary boundary segment is therefore $2(E/2) = E$. The formation energy of a single kink in the boundary also costs energy E. A double kink costs energy $2E$, a triple kink $3E$, etc. (see Figure 3 for a schematic diagram). The partition function for an elementary boundary segment unit with length a is given by summing over all possible boundary configurations:[31,33,34]

dx.doi.org/10.1021/la400082z | Langmuir 2013, 29, 3662−3667

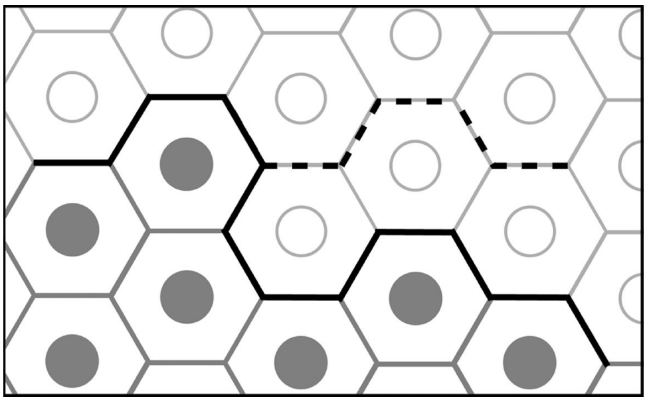

Figure 3. (—) Schematic diagram of a domain boundary of a triangular lattice with isotropic nearest-neighbor interaction (E). The nearest-neighbor distance of the atoms is a. The length of an elementary boundary segment along the horizontal direction is $a\sqrt{3}/2$. (---) Domain boundary at $T = 0$ K.

$$\begin{aligned} Z &= \sum_i e^{-E_i/k_bT} \\ &= 2e^{-E/k_bT} + 2e^{-2E/k_bT} + ... \\ &= \sum_{n=1}^{\infty} 2e^{-nE/k_bT} \\ &= \frac{2}{e^{E/k_bT} - 1} \end{aligned} \tag{1}$$

The factor of 2 comes from the degeneracy of the pathways since kinks can point to the right or to the left. The boundary free energy per unit length $a = a_{nn}\sqrt{3}/2$ is given by

$$F = -k_bT \ln\left(\frac{2}{e^{E/k_bT} - 1}\right) \tag{2}$$

The order−disorder phase transition temperature can be found by setting the boundary free energy equal to 0, resulting in $T_R = E/(k_b \ln 3)$. As shown by Wannier,[35] this is precisely the phase transition temperature of the isotropic triangular 2D Ising spin−lattice.

The probability to find a kink depends on its length: the longer the kink, the lower its probability of occurrence. In order to analyze the thermally induced meandering of the boundaries, it is very helpful to introduce the mean-square kink length,[36] $\langle n^2 \rangle$, which is defined as

$$\begin{aligned} \langle n^2 \rangle &= \sum_{n=-\infty}^{\infty} n^2 P_n \\ &= \frac{\sum_{n=-\infty}^{\infty} 2n^2 e^{-nE/k_bT}}{\sum_{n=-\infty}^{\infty} 2e^{-nE/k_bT}} \\ &= \frac{e^{-E/k_bT}(e^{-E/k_bT} + 1)}{(1 - e^{-E/k_bT})^2} \end{aligned} \tag{3}$$

where P_n is the probability of finding a kink with length n, The summation runs over all the possible kink configurations. The mean-square kink length is the expectation value of the square kink length and can be considered as the diffusivity of the domain boundary.[37,38] The value $\langle n^2 \rangle$ can be immediately extracted from the distribution of kinks and kink lengths. At the phase transition temperature, $e^{-E/k_bT_R} = {}^1/_3$ and thus the mean-square kink length will be exactly 1 at the phase transition temperature.

The mean-square displacement or deviation−deviation correlation function of a boundary is given by[35]

$$\langle (h_r - h_0)^2 \rangle = \langle n^2 \rangle \frac{r}{a} \tag{4}$$

where r is the position along the boundary and h_r the deviation measured in a direction perpendicular to the boundary. The mean-square displacement, $\langle (h_r - h_0)^2 \rangle$, can be extracted from the STM images by determining the mean-square displacement of the step with respect to its "mean" direction. This mean direction is always aligned along one of the three high-symmetry directions of the underlying Au(111) substrate (see Figure 1). We emphasize here that there is no need to measure the domain wall position, r, and the mean-square displacement with atomic or molecular resolution, in units of a. Here we have chosen to measure these positions in nanometers, which is perfectly fine since the mean-square displacement scales linearly with the position measured along the domain wall (see Figure 4). The slope of the curve is just the mean-square kink length, $\langle n^2 \rangle$.

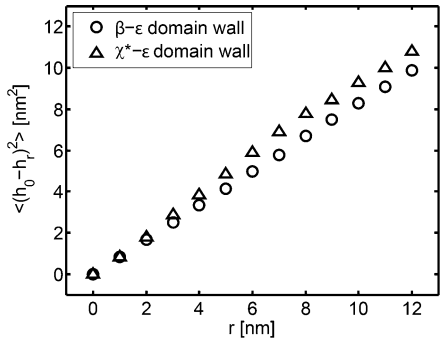

Figure 4. Mean-square displacement, $\langle (h_0 - h_r)^2 \rangle$, of (○) β−ε domain boundary and (△) χ^*−ε domain boundary versus the position measured r along the domain boundary.

In Figure 4 a plot of the mean-square displacement as a function of r for both the β and χ^* domain boundaries is shown. The mean-square length, $\langle n^2 \rangle$, at room temperature is 0.83 and 0.97 for β and χ^* domain boundaries, respectively. The experimental data reveals an almost exact linear relationship, which implies a random distribution of kinks in the domain boundaries. In addition, the slopes of both curves are a little smaller than 1, suggesting that the actual temperature is very close to the phase transition temperatures. From the slopes in Figure 4 we extract nearest-neighbor interaction energies of E_β = 30 meV/nm and E_{χ^*} = 28 meV/nm. The boundary free energies are plotted in Figure 5. The phase transition temperatures are 325 and 295 K for β and χ^* domain boundaries, respectively. The phase transition temperature of the χ^* phase is close to room temperature, which means that at room temperature domain boundaries can easily be generated since their formation free energy is almost 0. For the β phase the phase transition temperature is somewhat higher, and therefore this phase appears more stable at room temperature. These findings are consistent with previous observations of Poirier[22] and Toerker et al.[27] Both observed that the χ^* phase is metastable at room temperature, while the β phase remains stable at temperatures up to 325 K.

dx.doi.org/10.1021/la400082z | Langmuir 2013, 29, 3662−3667

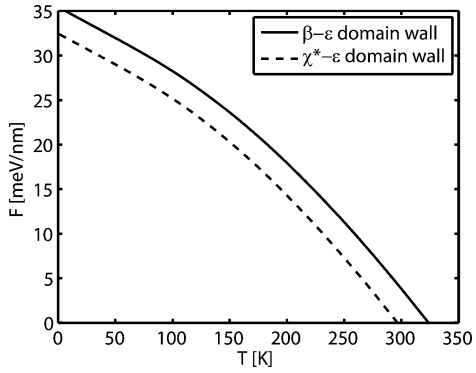

Figure 5. Domain boundary free energies of (—) β–ε domain boundary and (---) χ^*–ε domain boundary versus temperature. The phase transition temperatures are 295 and 325 K, respectively.

CONCLUSION

In summary, we have studied the domain boundaries between various low-coverage ordered phases (β and χ^*) and the disordered phase (ε) of a decanethiolate self-assembled monolayer on Au(111) using scanning tunneling microscopy. By analyzing the thermally induced meandering of the domain boundaries, we are able to determine the domain boundary free energies and extract the phase diagram of this system. The χ^*–ε and β–ε domain boundaries vanishes at 295 and 325 K, respectively. These findings are in very good agreement with the phase diagram put forward by Poirier et al.[1]

AUTHOR INFORMATION

Corresponding Author

*E-mail h.j.w.zandvliet@utwente.nl.

Author Contributions

[§]K.S. and H.W. contributed equally to this work.

Notes

The authors declare no competing financial interest.

ACKNOWLEDGMENTS

We thank the Stichting voor Fundamenteel Onderzoek der Materie (FOM) and the Strategic Research Orientation "Enabling Technologies" of the MESA+ Institute for Nanotechnology for financial support.

REFERENCES

(1) Poirier, G. E.; Fitts, W. P.; White, J. M. Two-dimensional phase diagram of decanethiol on Au(111). *Langmuir* **2001**, *17* (4), 1176–1183.

(2) Tamm, L. K.; McConnell, H. M. Supported phospholipid bilayers. *Biophys. J.* **1985**, *47* (1), 105–113.

(3) Faul, C. F. J.; Antonietti, M. Ionic self-assembly: Facile synthesis of supramolecular materials. *Adv. Mater.* **2003**, *15* (9), 673–683.

(4) Ulman, A. Formation and structure of self-assembled monolayers. *Chem. Rev.* **1996**, *96* (4), 1533–1554.

(5) Schreiber, F. Structure and growth of self-assembling monolayers. *Prog. Surf. Sci.* **2000**, *65* (5–8), 151–256.

(6) Lee, S.; Puck, A.; Graupe, M.; Colorado, R.; Shon, Y. S.; Lee, T. R.; Perry, S. S. Structure, wettability, and frictional properties of phenyl-terminated self-assembled monolayers on gold. *Langmuir* **2001**, *17* (23), 7364–7370.

(7) Zhang, S. Fabrication of nanomaterials through molecular self-assembly. *Nat. Biotechnol.* **2003**, *21*, 1171–1178.

(8) Dubois, L. H.; Zegarski, B. R.; Nuzzo, R. G. Molecular ordering of organosulfur compounds on Au(111) and Au(100): Adsorption from solution and in ultra-high vacuum. *J. Chem. Phys.* **1993**, *98* (1), 678–688.

(9) Fukuma, T.; Kobayashi, K.; Horiuchi, T.; Yamada, H.; Matsushige, K. Alkanethiol self-assembled monolayers on Au(111) surfaces investigated by non-contact AFM. *Appl. Phys. A: Mater. Sci. Process.* **2001**, *72*, S109–S112.

(10) Schreiber, F.; Eberhardt, A.; Leung, T. Y. B.; Schwartz, P.; Wetterer, S. M.; Lavrich, D. J.; Berman, L.; Fenter, P.; Eisenberger, P.; Scoles, G. Adsorption mechanisms, structures, and growth regimes of an archetypal self-assembled system: Decanethiol on Au(111). *Phys. Rev. B* **1998**, *57*, 12476–12481.

(11) Yamada, R.; Uosaki, K. In situ scanning tunneling microscopy observation of the self-assembly process of alkanethiols on gold(111) in solution. *Langmuir* **1998**, *14* (4), 855–861.

(12) Vericat, C.; Vela, M. E.; Salvarezza, R. C. Self-assembled monolayers of alkanethiols on Au(111): Surface structures, defects and dynamics. *Phys. Chem. Chem. Phys.* **2005**, *7* (18), 3258–3268.

(13) Qian, Y.; Yang, G.; Yu, J.; Jung, T. A.; Liu, G. Structures of annealed decanethiol self-assembled monolayers on Au(111): an ultrahigh vacuum scanning tunneling microscopy study. *Langmuir* **2003**, *19* (15), 6056–6065.

(14) Love, J. C.; Estroff, L. A.; Kriebel, J. K.; Nuzzo, R. G.; Whitesides, G. M. Self-assembled monolayers of thiolates on metals as a form of nanotechnology. *Chem. Rev.* **2005**, *105* (4), 1103–1170.

(15) Vericat, C.; Vela, M. E.; Benitez, G.; Carro, P.; Salvarezza, R. C. Self-assembled monolayers of thiols and dithiols on gold: New challenges for a well-known system. *Chem. Soc. Rev.* **2010**, *39* (5), 1805–1834.

(16) Aviram, A.; Ratner, M. A. Molecular rectifiers. *Chem. Phys. Lett.* **1974**, *29*, 277–283.

(17) Donhauser, Z. J.; Mantooth, B. A.; Kelly, K. F.; Bumm, L. A.; Monnell, J. D.; Stapleton, J. J.; Price, D. W.; Rawlett, A. M.; Allara, D. L.; Tour, J. M.; Weiss, P. S. Conductance switching in single molecules through conformational changes. *Science* **2001**, *292* (5525), 2303–2307.

(18) Teran Arce, F.; Vela, M. E.; Salvarezza, R. C.; Arvia, A. J. The dynamic behavior of butanethiol and dodecanethiol adsorbates on Au(111) terraces. *J. Chem. Phys.* **1998**, *109*, 5703–5706.

(19) Picraux, L. B.; Zangmeister, C. D.; Batteas, J. D. Preparation and structure of a low-density, flat-lying decanethiol monolayer from the densely packed upright monolayer on gold. *Langmuir* **2006**, *22* (1), 174–180.

(20) Fitts, W. P.; White, J. M.; Poirier, G. E. Low-coverage decanethiolate structure on Au(111): Substrate effects. *Langmuir* **2002**, *22* (5), 1561–1566.

(21) Sellers, H.; Ulman, A.; Shnidman, Y.; Eilers, J. E. Structure and binding of alkanethiolates on gold and silver surfaces: Implications for self-assembled monolayers. *J. Am. Chem. Soc.* **1993**, *115* (21), 9389–9401.

(22) Poirier, G. E. Coverage-dependent phases and phase stability of decanethiol on Au(111). *Langmuir* **1999**, *15*, 1167–1175.

(23) Poirier, G. E.; Tarlov, M. J. The c(4 × 2) superlattice of *n*-alkanethiol monolayers self-assembled on Au(111). *Langmuir* **1994**, *10*, 2853–2856.

(24) Poirier, G. E. Mechanism of formation of Au vacancy islands in alkanethiol monolayers on Au(111). *Langmuir* **1997**, *13*, 2019–2026.

(25) Staub, R.; Toerker, M.; Fritz, T.; Schmitz-Hbsch, T.; Sellam, F.; Leo, K. Flat lying pin-stripe phase of decanethiol self-assembled monolayers on Au(111). *Langmuir* **1998**, *14* (23), 6693–6698.

(26) Gerlach, R.; Polanski, G.; Rubahn, H. G. Structural manipulation of ultrathin organic films on metal surfaces: The case of decanethiol/Au(111). *Appl. Phys. A: Mater. Sci. Process.* **1997**, *65*, 375–377.

(27) Toerker, M.; Staub, R.; Fritz, T.; Schmitz-Hbsch, T.; Sellam, F.; Leo, K. Annualed decanethiol monolayers on Au(111): Intermediate phases between structures with high and low molecular surface denisty. *Surf. Sci.* **2000**, *445*, 100–108.

(28) Li, S. S.; Xu, L. P.; Wan, L. J.; Wang, S. T.; Jiang, L. Time-dependent organization and wettability of decanethiol self-assembled

monolayer on Au(111) investigated with STM. *J. Phys. Chem. B* **2006**, *110* (4), 1794−1799.
(29) Fitts, W. P.; White, J. M.; Poirier, G. E. Thermodynamics of decanethiol adsorption on Au(111): Extension to 0 °C. *Langmuir* **2002**, *18*, 2096−2102.
(30) Schoenenberg, C.; Sondag-Huethorst, J. A. M.; Jorritsma, J.; Fokkink, L. G. J. What are the "holes" in self-assembled monolayers of alkanethiols on gold? *Langmuir* **1994**, *10*, 611−614.
(31) Burton, W. K.; Cabrera, N.; Frank, F. C. The growth of crystals and the equilibrium structure of their surfaces. *Philos. Trans. R. Soc. A* **1951**, *243* (866), 299−358.
(32) Kole, P. R.; de Vries, R. J.; Poelsema, B.; Zandvliet, H. J. W. Free energies of steps on (111) fcc surfaces. *Solid State Commun.* **2005**, *136* (6), 356−359.
(33) Zandvliet, H. J. W. Energetics of Si(001). *Rev. Mod. Phys.* **2000**, *72* (2), 593−602.
(34) Zandvliet, H. J. W. The Ge(001) surface. *Phys. Rep.* **2003**, *388*, 1−40.
(35) Wannier, G. H. The statistical problem in cooperative phenomena. *Rev. Mod. Phys.* **1945**, *17* (1), 50−60.
(36) Zandvliet, H. J. W.; Elswijk, H. B. Morphology of monatomic step edges on vicinal Si(001). *Phys. Rev. B* **1993**, *48* (19), 14269−14275.
(37) Zandvliet, H. J. W. Determination of Ge(001) step free energies. *Phys. Rev. B* **2000**, *61*, 9972−9974.
(38) Bartelt, N. C.; Einstein, T. L.; Williams, E. D. The role of step collisions on diffraction from vicinal surfaces. *Surf. Sci.* **1992**, *276* (1−3), 308−324.